

POLARIZED LINE FORMATION WITH J -STATE INTERFERENCE IN THE PRESENCE OF MAGNETIC FIELDS. I. PARTIAL FREQUENCY REDISTRIBUTION IN THE COLLISIONLESS REGIME

H. N. SMITHA¹, M. SAMPOORNA¹, K. N. NAGENDRA¹, AND J. O. STENFLO^{2,3}

¹ Indian Institute of Astrophysics, Koramangala, Bangalore, India; smithahn@iiap.res.in, sampoorna@iiap.res.in, knn@iiap.res.in

² Institute of Astronomy, ETH Zürich, CH-8092 Zürich, Switzerland; stenflo@astro.phys.ethz.ch

³ Istituto Ricerche Solari Locarno, Via Patocchi, 6605 Locarno-Monti, Switzerland

Received 2011 January 1; accepted 2011 March 10; published 2011 April 27

ABSTRACT

Quantum interference phenomena play a fundamental role in astrophysical spectra that are formed by coherent scattering processes. Here we derive a partial frequency redistribution (PRD) matrix that includes J -state interference in the presence of magnetic fields of arbitrary strength. The paper focuses on PRD in the collisionless regime, which in the traditional PRD terminology is referred to as Hummer's type-II scattering. By limiting the treatment to the linear Zeeman regime, for which the Zeeman splitting is much smaller than the fine-structure splitting, it is possible to formulate analytical expressions for the PRD matrices. In the special case of non-magnetic scattering we recover the redistribution matrix derived from an independent quantum electrodynamic formulation based on the metalevel theory.

Key words: atomic processes – line: profiles – magnetic fields – polarization – scattering – Sun: atmosphere

1. INTRODUCTION

The linearly polarized spectrum (the second solar spectrum) of the Sun, formed due to coherent scattering processes, is a fingerprint of physics of scattering (see Stenflo & Keller 1996, 1997). For example, Stenflo (1980) showed for the first time that the scattering polarization signatures that he observed for the solar Ca II H and K lines could only be explained when J -state interference between the $J = 1/2$ and $J = 3/2$ levels was taken into account. The interpretation of second solar spectrum requires the use of advanced theories of scattering in the presence of magnetic fields. The Rayleigh (non-magnetic) scattering phase matrix for a $J = 0 \rightarrow 1 \rightarrow 0$ scattering transition was derived by Chandrasekhar (1950) using classical electrodynamics. The phase matrix for arbitrary (namely, a $J_a \rightarrow J_b \rightarrow J_a$) scattering transition was derived by Hamilton (1947) using quantum mechanics. A classical electrodynamic expression of the Hanle phase matrix for polarized light scattering on atoms in the presence of weak magnetic fields was given by Stenflo (1978). The quantum electrodynamic (QED) theory of polarized scattering on atoms in the presence of arbitrary strength magnetic fields was formulated in Bommier & Sahal-Bréchet (1978) and Landi Degl'Innocenti (1983, 1984, 1985), under the assumption of complete frequency redistribution (CRD).

The interpretation of observed linear polarization in resonance lines often requires the use of partial frequency redistribution (PRD) in scattering. The problem of frequency redistribution in resonance lines for non-magnetic and weak magnetic field cases was formulated by Omont et al. (1972, 1973) using a quantum approach. Based on this work, Domke & Hubeny (1988) derived an explicit form of the polarized PRD matrix for resonance scattering. Using a master equation theory, Bommier (1997a, 1997b) derived the polarized PRD matrices for scattering in non-magnetic and arbitrary strength magnetic fields. Her theory can handle an arbitrary scattering transition $J_a \rightarrow J_b \rightarrow J_a$, with J_a and J_b being the angular momentum quantum numbers of the lower and the upper states, respectively. The lower level in this theory is assumed to be unpolarized.

A classical PRD theory for the scattering of polarized radiation in the presence of arbitrary strength magnetic fields

was developed by Bommier & Stenflo (1999). They solved the time-dependent oscillator equation, in combination with a classical model for collisions (see Stenflo 1994, Chapter 10). However, Bommier & Stenflo (1999) present the polarized PRD matrices in the atomic rest frame. The corresponding laboratory frame redistribution matrices were derived in Sampoorna et al. (2007a, hereafter P1). For the particular case of a $J = 0 \rightarrow 1 \rightarrow 0$ scattering transition, Sampoorna et al. (2007b, hereafter P2) showed that the QED theory of Bommier (1997b) and the classical oscillator theory give identical results. Following the suggestion given in Section 5 of P1, Sampoorna (2011) has extended the classical theory to treat atomic transitions with arbitrary J -quantum numbers. This extension proceeds in a phenomenological way, drawing on the analogy between the Kramers–Heisenberg scattering amplitude for line scattering in quantum mechanics and the Jones matrix for classical polarized scattering. The PRD matrices derived from such a semi-classical approach are in agreement with those derived by Bommier (1997b).

Stenflo (1980, 1994, 1997) formulated the quantum theory of J -state interference for frequency coherent scattering. A QED theory for the multi-term atom (that includes also the J -state interference) under the assumption of CRD is given in Landi Degl'Innocenti & Landolfi (2004, hereafter LL04). A metalevel theory (also including J -state interference) has been formulated by Landi Degl'Innocenti et al. (1997) to deal with PRD problems in the presence of magnetic fields of arbitrary strength in the absence of collisions.

In the present paper, based on the Kramers–Heisenberg scattering formula, we derive polarized PRD matrices including the J -state interference. Here we restrict our attention to scattering in the absence of collisions (the so-called type-II scattering of Hummer 1962). Our formulation however has the advantage that it allows elastic collisions to be taken into account by following an approach similar to that described in P1, in the context of m -state interference phenomenon. We consider an $L_a \rightarrow L_b \rightarrow L_f$ scattering transition, where L_a , L_b , and L_f denote the orbital angular momentum quantum numbers of the initial, intermediate, and final levels, respectively, but limit ourselves here to the case of resonance scattering with common

initial and final states, $L_a = L_f$. According to the terminology of LL04 (p. 580), this is a two-term atom.

Due to L – S coupling, a given (L, S) state splits into several J -states, with $|L - S| \leq J \leq |L + S|$. Here we account for interference between the J_b -states belonging to a given excited L_b -state. This includes the interference between the magnetic substates of different J_b -states. However, the present treatment is limited to the regime where the Zeeman splitting is much smaller than the fine-structure splitting. Therefore, the Paschen–Back regime is not covered and the level crossings are not dealt with. Thus, in the linear Zeeman regime of relatively weak fields, the interference between magnetic substates belonging to different J -states takes place mainly in the line wings, outside the Doppler cores. The Paschen–Back theory that covers the regime of relatively strong fields is given in LL04.

In Section 2 we recall the expressions of the Kramers–Heisenberg formula and the Mueller scattering matrix. In Section 3 we derive the elements of the redistribution matrix in both the atomic and the laboratory frames. In Section 4 we rewrite the redistribution matrix derived in Section 3 in terms of the irreducible spherical tensors. The Stokes profiles obtained for single scattering on an $L = 0 \rightarrow 1 \rightarrow 0$ transition with $S = 1/2$ are discussed in detail in Section 5. The concluding remarks are given in Section 6.

2. KRAMERS–HEISENBERG FORMULA AND THE MUELLER SCATTERING MATRIX

The complex probability amplitude for scattering from a given initial magnetic substate a to a final substate f via all possible intermediate substates b is given by the Kramers–Heisenberg formula (see Stenflo 1998)

$$w_{\alpha\beta} \sim \sum_b \frac{\langle f | \mathbf{r} \cdot \mathbf{e}_\alpha | b \rangle \langle b | \mathbf{r} \cdot \mathbf{e}_\beta | a \rangle}{\omega_{bf} - \omega - i\gamma/2}, \quad (1)$$

where $\omega = 2\pi\xi$ is the angular frequency of the scattered radiation in the atomic rest frame, $\hbar\omega_{bf}$ is the energy difference between the excited and final states, and γ is the damping constant that accounts for the broadening of the excited state, while the initial and final states are assumed to be infinitely sharp. The damping parameter is assumed to be same for all the magnetic substates of the excited state. The matrix elements appearing in Equation (1) can be expanded using the Wigner–Eckart theorem (see Stenflo 1994, pp. 145 and 199). This gives us

$$\begin{aligned} w_{\alpha\beta}(J_f \mu_f J_a \mu_a) &\sim \sum_{J_b \mu_b} (-1)^{q-q'} \sqrt{(2J_a+1)(2J_f+1)(2J_b+1)} \\ &\times (2L_a+1) \begin{Bmatrix} L_a & L_b & 1 \\ J_b & J_f & S \end{Bmatrix} \begin{Bmatrix} L_a & L_b & 1 \\ J_b & J_a & S \end{Bmatrix} \\ &\times \begin{pmatrix} J_b & J_a & 1 \\ -\mu_b & \mu_a & -q' \end{pmatrix} \begin{pmatrix} J_b & J_f & 1 \\ -\mu_b & \mu_f & -q \end{pmatrix} \\ &\times \Phi_\gamma(v_{J_b \mu_b J_f \mu_f} - \xi) \varepsilon_q^{\alpha*} \varepsilon_{q'}^\beta, \end{aligned} \quad (2)$$

where μ_b represents the magnetic substates of the upper level b with total angular momentum quantum number J_b , orbital angular momentum quantum number L_b , and spin S . The total angular momentum quantum numbers of the initial and final states are J_a and J_f with orbital angular momentum quantum number L_a , spin S , and magnetic substates μ_a and μ_f , respectively. The quantities ε are the geometrical factors (see

Equations (2) and (27) of Stenflo 1998) with α and β denoting the outgoing and incoming rays, respectively. In Equation (2), q and q' satisfy

$$q = \mu_f - \mu_b; \quad q' = \mu_a - \mu_b. \quad (3)$$

The frequency-normalized profile function is given by

$$\Phi_\gamma(v_{J_b \mu_b J_f \mu_f} - \xi) = \frac{1/(\pi i)}{v_{J_b \mu_b J_f \mu_f} - \xi - i\gamma/(4\pi)}, \quad (4)$$

where

$$v_{J_b \mu_b J_f \mu_f} = v_{J_b J_f} + (g_b \mu_b - g_f \mu_f) v_L. \quad (5)$$

Here, $h v_{J_b J_f}$ is the energy difference between the upper state J_b and lower state J_f in the absence of magnetic fields, $g_{b,f}$ are the Landé factors of the J_b and J_f states, and v_L is the Larmor frequency. Equation (2) refers to the frequency-coherent scattering case. The Mueller matrix \mathbf{M} that describes the transformation from the incident to the scattered Stokes vector is of the form (see Equation (7) of Stenflo 1998)

$$\mathbf{M} = \mathbf{T} \mathbf{W} \mathbf{T}^{-1}, \quad (6)$$

where

$$\mathbf{W} = \sum_{J_a \mu_a} \rho_{\mu_a \mu_a} \sum_{J_f \mu_f} \mathbf{w}(J_f \mu_f J_a \mu_a) \otimes \mathbf{w}^*(J_f \mu_f J_a \mu_a). \quad (7)$$

The symbol \otimes stands for the tensor product. $\rho_{\mu_a \mu_a}$ represents the relative populations of the initial magnetic substates μ_a (diagonal elements of the density matrix for the initial state, normalized such that the sum over $\rho_{\mu_a \mu_a}$ is unity). Without initial-state polarization, all the $\rho_{\mu_a \mu_a}$ are equal and can therefore be absorbed in the normalization constant for the Mueller matrix \mathbf{M} . In Equation (6), \mathbf{T} and \mathbf{T}^{-1} are purely mathematical transformation matrices, and their explicit forms are given in Equation (9) of Stenflo (1998).

3. COLLISIONLESS REDISTRIBUTION MATRIX INCLUDING THE J -STATE INTERFERENCE

The matrix form of the tensor product $\mathbf{w}(J_f \mu_f J_a \mu_a) \otimes \mathbf{w}^*(J_f \mu_f J_a \mu_a)$ in Equation (7), which is needed for the computation of the redistribution matrix, is given by Equation (10) of Stenflo (1998). It contains bilinear products like $w_{\alpha\beta}(J_f \mu_f J_a \mu_a) w_{\alpha'\beta'}^*(J_f \mu_f J_a \mu_a)$. The profile function $\Phi_\gamma(v_{J_b \mu_b J_f \mu_f} - \xi)$ appearing in Equation (2) for outgoing frequency (ξ) may be replaced by $\Phi_\gamma'(v_{J_b \mu_b J_a \mu_a} - \xi')$ for incoming frequency (ξ'), through an application of energy conservation (see Equation (9.10) of Stenflo 1994). The profile function $\Phi_\gamma'(v_{J_b \mu_b J_a \mu_a} - \xi')$ is given by Equation (4) with ξ replaced by ξ' , while $v_{J_b \mu_b J_f \mu_f}$ is replaced by $v_{J_b \mu_b J_a \mu_a}$ which is defined similar to Equation (5). Thus, the bilinear product $w_{\alpha\beta}(J_f \mu_f J_a \mu_a) w_{\alpha'\beta'}^*(J_f \mu_f J_a \mu_a)$ can be written in the atomic frame as

$$\begin{aligned} w_{\alpha\beta}(J_f \mu_f J_a \mu_a) w_{\alpha'\beta'}^*(J_f \mu_f J_a \mu_a) &\sim \sum_{J_b \mu_b J_b' \mu_b'} (-1)^{q-q'} \\ &\times (-1)^{q''-q'''} \varepsilon_q^{\alpha*} \varepsilon_{q'}^{\alpha'} \varepsilon_{q''}^\beta \varepsilon_{q'''}^{\beta'*} \cos \beta_{J_b' \mu_b' J_b \mu_b} e^{i\beta_{J_b' \mu_b' J_b \mu_b}} \\ &\times \Phi_{J_b \mu_b J_b' \mu_b' J_a \mu_a}^\gamma(\xi') \delta(\xi - \xi' - v_{J_a \mu_a J_f \mu_f}) (2J_a+1)(2J_f+1) \\ &\times (2J_b+1)(2J_b'+1)(2L_a+1)^2 \begin{Bmatrix} L_a & L_b & 1 \\ J_b & J_f & S \end{Bmatrix} \begin{Bmatrix} L_a & L_b & 1 \\ J_b & J_a & S \end{Bmatrix} \end{aligned}$$

$$\begin{aligned}
 & \times \begin{Bmatrix} L_a & L_b & 1 \\ J_{b'} & J_f & S \end{Bmatrix} \begin{Bmatrix} L_a & L_b & 1 \\ J_{b'} & J_a & S \end{Bmatrix} \begin{pmatrix} J_b & J_a & 1 \\ -\mu_b & \mu_a & -q' \end{pmatrix} \\
 & \times \begin{pmatrix} J_{b'} & J_a & 1 \\ -\mu_{b'} & \mu_a & -q''' \end{pmatrix} \begin{pmatrix} J_b & J_f & 1 \\ -\mu_b & \mu_f & -q \end{pmatrix} \\
 & \times \begin{pmatrix} J_{b'} & J_f & 1 \\ -\mu_{b'} & \mu_f & -q'' \end{pmatrix}. \quad (8)
 \end{aligned}$$

In the above equation we have introduced the delta-function term $\delta(\xi - \xi' - \nu_{J_a\mu_a J_f\mu_f})$, which is simply the statement of energy conservation (see Equations (9.7) and (9.10) of Stenflo 1994). This term is essential as we are dealing with type-II scattering which represents coherent scattering in the atom's rest frame. The $\nu_{J_a\mu_a J_f\mu_f}$ appearing in the delta function is given by

$$\nu_{J_a\mu_a J_f\mu_f} = \nu_{J_a J_f} + (g_a \mu_a - g_f \mu_f) \nu_L, \quad (9)$$

where $h\nu_{J_a J_f}$ is the energy difference between the states J_a and J_f in the absence of a magnetic field. The angle $\beta_{J_{b'}\mu_{b'} J_b\mu_b}$ (arising due to the combined effects of the J -state and m -state interferences) is defined by

$$\tan \beta_{J_{b'}\mu_{b'} J_b\mu_b} = \frac{\omega_{J_{b'} J_b} + (g_{b'} \mu_{b'} - g_b \mu_b) \omega_L}{\gamma}, \quad (10)$$

where $h\omega_{J_{b'} J_b}$ represents the energy difference between the $J_{b'}$ and J_b states in the absence of a magnetic field. When $J_b = J_{b'}$, the angle $\beta_{J_{b'}\mu_{b'} J_b\mu_b}$ describes the m -state interference (see Stenflo 1994, p. 87) and when $J_b \neq J_{b'}$, it characterizes the J -state interference. In the present paper we limit the treatment to the linear Zeeman regime, in which the Zeeman splitting is much smaller than the fine-structure splitting. When $J_b \neq J_{b'}$, the contribution from the second term with ω_L in Equation (10) to the angle $\beta_{J_{b'}\mu_{b'} J_b\mu_b}$ can therefore be ignored, because it is insignificant in comparison with the first term.

The ‘‘generalized profile function’’ is defined as

$$\begin{aligned}
 \Phi_{J_b\mu_b J_{b'}\mu_{b'} J_f\mu_f}^\gamma(\xi) &= \frac{1}{2} [\Phi_\gamma(\nu_{J_b\mu_b J_f\mu_f} - \xi) \\
 &+ \Phi_\gamma^*(\nu_{J_{b'}\mu_{b'} J_f\mu_f} - \xi)]. \quad (11)
 \end{aligned}$$

When deriving Equation (8), we have made use of the following relation:

$$\begin{aligned}
 & \Phi_\gamma(\nu_{J_b\mu_b J_f\mu_f} - \xi) \Phi_\gamma^*(\nu_{J_{b'}\mu_{b'} J_f\mu_f} - \xi) \\
 &= \frac{4}{\gamma - i(\omega_{J_{b'}\mu_{b'} J_f\mu_f} - \omega_{J_b\mu_b J_f\mu_f})} \Phi_{J_b\mu_b J_{b'}\mu_{b'} J_f\mu_f}^\gamma(\xi). \quad (12)
 \end{aligned}$$

Equation (8) can be transformed to the laboratory frame following exactly the same steps as described in Section 2.2 of P1 (see also Section 3.3 of Bommier 1997b). Thus, in the laboratory frame, the bilinear product $w_{\alpha\beta}(J_f\mu_f J_a\mu_a) w_{\alpha'\beta'}^*(J_f\mu_f J_a\mu_a)$ is given by Equation (8), but with the following replacement:

$$\begin{aligned}
 & \Phi_{J_b\mu_b J_{b'}\mu_{b'} J_a\mu_a}^\gamma(\xi') \delta(\xi - \xi' - \nu_{J_a\mu_a J_f\mu_f}) \longrightarrow \\
 & [(h_{J_b\mu_b, J_{b'}\mu_{b'}}^\Pi)_{J_a\mu_a J_f\mu_f} + i (f_{J_b\mu_b, J_{b'}\mu_{b'}}^\Pi)_{J_a\mu_a J_f\mu_f}], \quad (13)
 \end{aligned}$$

where

$$(h_{J_b\mu_b, J_{b'}\mu_{b'}}^\Pi)_{J_a\mu_a J_f\mu_f} = \frac{1}{2} [R_{J_b\mu_b J_a\mu_a J_f\mu_f}^{\Pi, H} + R_{J_{b'}\mu_{b'} J_a\mu_a J_f\mu_f}^{\Pi, H}], \quad (14)$$

$$(f_{J_b\mu_b, J_{b'}\mu_{b'}}^\Pi)_{J_a\mu_a J_f\mu_f} = \frac{1}{2} [R_{J_{b'}\mu_{b'} J_a\mu_a J_f\mu_f}^{\Pi, F} - R_{J_b\mu_b J_a\mu_a J_f\mu_f}^{\Pi, F}], \quad (15)$$

and the magnetic redistribution functions of type II are given by

$$\begin{aligned}
 & R_{J_b\mu_b J_a\mu_a J_f\mu_f}^{\Pi, H}(x_{ba}, x'_{ba}, \Theta) = \frac{1}{\pi \sin \Theta} \\
 & \times \exp \left\{ - \left[\frac{x_{ba} - x'_{ba} + x_{J_a\mu_a J_f\mu_f}}{2 \sin(\Theta/2)} \right]^2 \right\} \\
 & \times H \left(\frac{a}{\cos(\Theta/2)}, \frac{\nu_{J_b\mu_b J_a\mu_a} + \nu'_{J_b\mu_b J_a\mu_a} + x_{J_a\mu_a J_f\mu_f}}{2 \cos(\Theta/2)} \right) \quad (16)
 \end{aligned}$$

and

$$\begin{aligned}
 & R_{J_b\mu_b J_a\mu_a J_f\mu_f}^{\Pi, F}(x_{ba}, x'_{ba}, \Theta) = \frac{1}{\pi \sin \Theta} \\
 & \times \exp \left\{ - \left[\frac{x_{ba} - x'_{ba} + x_{J_a\mu_a J_f\mu_f}}{2 \sin(\Theta/2)} \right]^2 \right\} \\
 & \times 2F \left(\frac{a}{\cos(\Theta/2)}, \frac{\nu_{J_b\mu_b J_a\mu_a} + \nu'_{J_b\mu_b J_a\mu_a} + x_{J_a\mu_a J_f\mu_f}}{2 \cos(\Theta/2)} \right). \quad (17)
 \end{aligned}$$

In the above equations, $H(a, x)$ and $F(a, x)$ are the Voigt and Faraday–Voigt functions defined by

$$\begin{aligned}
 H(a, x) &= \frac{a}{\pi} \int_{-\infty}^{+\infty} \frac{e^{-y^2} dy}{(x-y)^2 + a^2}; \\
 F(a, x) &= \frac{1}{2\pi} \int_{-\infty}^{+\infty} \frac{e^{-y^2} (x-y) dy}{(x-y)^2 + a^2}. \quad (18)
 \end{aligned}$$

The scattering angle between the incident and scattered rays is denoted by Θ (see Figure 1). The dimensionless quantities appearing in Equations (16) and (17) are given by

$$\begin{aligned}
 x_{ba} &= \frac{\nu_{0ba} - \nu}{\Delta\nu_D}; \quad a = \frac{\gamma}{4\pi\Delta\nu_D}; \quad x_{J_a\mu_a J_f\mu_f} = \frac{\nu_{J_a\mu_a J_f\mu_f}}{\Delta\nu_D}; \\
 \nu_{J_b\mu_b J_a\mu_a} &= x_{ba} + (g_b \mu_b - g_a \mu_a) \frac{\nu_L}{\Delta\nu_D}, \quad (19)
 \end{aligned}$$

where x_{ba} , a , and $\Delta\nu_D$ are the emission frequency, damping parameter, and Doppler width, respectively. We note that $(f_{J_b\mu_b, J_{b'}\mu_{b'}}^\Pi)_{J_a\mu_a J_f\mu_f}$ is zero when both $J_b = J_{b'}$ and $\mu_b = \mu_{b'}$. Substituting Equation (8) in Equations (6) and (7), we obtain the Hanle–Zeeman redistribution matrix with the J -state interference included appropriately.

4. THE REDISTRIBUTION MATRIX EXPRESSED IN TERMS OF IRREDUCIBLE SPHERICAL TENSORS

The irreducible tensors $\mathcal{T}_Q^K(i, \mathbf{n})$ have been introduced by Landi Degl’Innocenti (1984) to deal with problems in polarized radiative transfer. Here index i refers to the Stokes parameters ($i = 0, 1, 2, 3$), while $K = 0, 1, 2$ with $-K \leq Q \leq +K$. In the following we will express the redistribution matrix in terms of \mathcal{T}_Q^K , which allows it to be written as a sum of its multipolar (K) components. We will need this form in particular for the collisional redistribution matrix (type III). Furthermore, in the weak field limit the expansion in terms of \mathcal{T}_Q^K allows us to express the Stokes intensity and source vectors in terms of the

respective ‘‘cylindrically symmetric’’ irreducible components I_Q^K and S_Q^K (see Frisch 2007).

We start by expressing the equations given in Sections 2 and 3 in terms of the irreducible spherical tensors for polarimetry, following Appendix C of P2 (see also LL04). Using Equation (3.84) of Stenflo (1994) and Equations (C1) and (C2) of P2, we can express the electric field E_μ of the scattered ray as

$$\begin{aligned}
 E_\mu \sim & \sum_{\rho J_b \mu_b} (-1)^{q-q'} \sqrt{(2J_a+1)(2J_f+1)(2J_b+1)(2L_a+1)} \\
 & \times \begin{Bmatrix} L_a & L_b & 1 \\ J_b & J_f & S \end{Bmatrix} \begin{Bmatrix} L_a & L_b & 1 \\ J_b & J_a & S \end{Bmatrix} \begin{pmatrix} J_b & J_a & 1 \\ -\mu_b & \mu_a & -q' \end{pmatrix} \\
 & \times \begin{pmatrix} J_b & J_f & 1 \\ -\mu_b & \mu_f & -q \end{pmatrix} \Phi_\gamma(v_{J_b \mu_b J_f \mu_f} - \xi) \\
 & \times [e_\mu(\mathbf{n})]_{q'}^* [e_\rho(\mathbf{n}')]_{q'} E'_\rho,
 \end{aligned} \quad (20)$$

where E'_ρ is the electric field of the incident radiation, and indices μ and ρ take the values 1 and 2. The above equation is written in the basis defined in Equation (C3) of P2. The elements of the coherency matrix may be written as

$$I_{\mu\nu}^S \sim \sum_{J_a \mu_a J_f \mu_f} E_\mu E_\nu^*. \quad (21)$$

Substituting for E_μ in Equation (21), we obtain

$$I_{\mu\nu}^S \sim \sum_{\rho\sigma} T_{\mu\nu,\rho\sigma}^S(\xi, \mathbf{n}; \xi', \mathbf{n}', \mathbf{B}) I_{\rho\sigma}^S, \quad (22)$$

where

$$\begin{aligned}
 T_{\mu\nu,\rho\sigma}^S(\xi, \mathbf{n}; \xi', \mathbf{n}', \mathbf{B}) = & \sum_{J_a \mu_a J_f \mu_f J_b \mu_b J_{b'} \mu_{b'}} (-1)^{q-q'} \\
 & \times (-1)^{q''-q'''} \mathcal{E}_{qq''}^S(\mu, \nu, \mathbf{n}) \mathcal{E}_{q''q'''}^S(\sigma, \rho, \mathbf{n}') \cos\beta_{J_{b'} \mu_{b'} J_b \mu_b} \\
 & \times e^{i\beta_{J_{b'} \mu_{b'} J_b \mu_b}} \Phi'_{J_b \mu_b J_{b'} \mu_{b'} J_a \mu_a}(\xi') \delta(\xi - \xi' - v_{J_a \mu_a J_f \mu_f}) \\
 & \times (2J_a+1)(2J_f+1)(2J_b+1)(2J_{b'}+1)(2L_a+1)^2 \\
 & \times \begin{Bmatrix} L_a & L_b & 1 \\ J_b & J_f & S \end{Bmatrix} \begin{Bmatrix} L_a & L_b & 1 \\ J_b & J_a & S \end{Bmatrix} \begin{Bmatrix} L_a & L_b & 1 \\ J_{b'} & J_f & S \end{Bmatrix} \\
 & \times \begin{Bmatrix} L_a & L_b & 1 \\ J_{b'} & J_a & S \end{Bmatrix} \begin{pmatrix} J_b & J_a & 1 \\ -\mu_b & \mu_a & -q' \end{pmatrix} \begin{pmatrix} J_b & J_f & 1 \\ -\mu_b & \mu_f & -q \end{pmatrix} \\
 & \times \begin{pmatrix} J_{b'} & J_a & 1 \\ -\mu_{b'} & \mu_a & -q''' \end{pmatrix} \begin{pmatrix} J_{b'} & J_f & 1 \\ -\mu_{b'} & \mu_f & -q'' \end{pmatrix}.
 \end{aligned} \quad (23)$$

Here, $\mathcal{E}_{qq''}^S(\mu, \nu, \mathbf{n})$ is a reducible spherical tensor (see Equation (C6) of P2). The transformation to the Stokes vector formalism from the coherency matrix formalism is described in Appendix C of P2. The scattered Stokes vector in the laboratory frame is given by

$$S_i = \sum_{j=0}^3 \mathbf{R}_{ij}^{\text{II}}(x, \mathbf{n}; x', \mathbf{n}', \mathbf{B}) S'_j, \quad (24)$$

where the normalized type-II redistribution matrix in the laboratory frame (see Equation (13)) is given by

$$\begin{aligned}
 \mathbf{R}_{ij}^{\text{II}}(x, \mathbf{n}; x', \mathbf{n}', \mathbf{B}) = & \frac{3(2L_b+1)}{2S+1} \sum_{K' K'' Q J_a \mu_a J_f \mu_f J_b \mu_b J_{b'} \mu_{b'}} \\
 & \times \sqrt{(2K'+1)(2K''+1)(2J_a+1)(2J_f+1)(2J_b+1)(2J_{b'}+1)}
 \end{aligned}$$

$$\begin{aligned}
 & \times (-1)^{q''+q'+Q} \cos\beta_{J_{b'} \mu_{b'} J_b \mu_b} e^{i\beta_{J_{b'} \mu_{b'} J_b \mu_b}} \left[(h_{J_b \mu_b, J_{b'} \mu_{b'}}^{\text{II}})_{J_a \mu_a J_f \mu_f} \right. \\
 & + i (f_{J_b \mu_b, J_{b'} \mu_{b'}}^{\text{II}})_{J_a \mu_a J_f \mu_f} \left. \begin{pmatrix} J_b & J_a & 1 \\ -\mu_b & \mu_a & -q' \end{pmatrix} \begin{pmatrix} J_b & J_f & 1 \\ -\mu_b & \mu_f & -q \end{pmatrix} \right] \\
 & \times \begin{pmatrix} J_{b'} & J_a & 1 \\ -\mu_{b'} & \mu_a & -q''' \end{pmatrix} \begin{pmatrix} J_{b'} & J_f & 1 \\ -\mu_{b'} & \mu_f & -q'' \end{pmatrix} \begin{pmatrix} 1 & 1 & K'' \\ q & -q'' & -Q \end{pmatrix} \\
 & \times \begin{pmatrix} 1 & 1 & K' \\ q''' & -q' & Q \end{pmatrix} \begin{Bmatrix} L_a & L_b & 1 \\ J_b & J_f & S \end{Bmatrix} \begin{Bmatrix} L_a & L_b & 1 \\ J_b & J_a & S \end{Bmatrix} \\
 & \times \begin{Bmatrix} L_a & L_b & 1 \\ J_{b'} & J_f & S \end{Bmatrix} \begin{Bmatrix} L_a & L_b & 1 \\ J_{b'} & J_a & S \end{Bmatrix} (-1)^Q \mathcal{T}_{-Q}^{K''}(i, \mathbf{n}) \mathcal{T}_Q^{K'}(j, \mathbf{n}').
 \end{aligned} \quad (25)$$

In Section 5 we present the results computed using Equation (25). When the magnetic field is set to zero in Equation (25), it takes a particularly simple form given by

$$\begin{aligned}
 \mathbf{R}_{ij}^{\text{II}}(x, \mathbf{n}; x', \mathbf{n}') = & \frac{3(2L_b+1)}{2S+1} \\
 & \times \sum_{K Q J_a J_f J_b J_{b'}} (-1)^{J_f-J_a} \cos\beta_{J_{b'} J_b} e^{i\beta_{J_{b'} J_b}} \\
 & \times \left[(h_{J_b, J_{b'}}^{\text{II}})_{J_a J_f} + i (f_{J_b, J_{b'}}^{\text{II}})_{J_a J_f} \right] \\
 & \times (2J_a+1)(2J_f+1)(2J_b+1)(2J_{b'}+1) \\
 & \times \begin{Bmatrix} L_a & L_b & 1 \\ J_b & J_f & S \end{Bmatrix} \begin{Bmatrix} L_a & L_b & 1 \\ J_b & J_a & S \end{Bmatrix} \begin{Bmatrix} L_a & L_b & 1 \\ J_{b'} & J_f & S \end{Bmatrix} \\
 & \times \begin{Bmatrix} L_a & L_b & 1 \\ J_{b'} & J_a & S \end{Bmatrix} \begin{Bmatrix} 1 & 1 & K \\ J_{b'} & J_b & J_a \end{Bmatrix} \begin{Bmatrix} 1 & 1 & K \\ J_{b'} & J_b & J_f \end{Bmatrix} \\
 & \times (-1)^Q \mathcal{T}_Q^K(i, \mathbf{n}) \mathcal{T}_{-Q}^K(j, \mathbf{n}').
 \end{aligned} \quad (26)$$

The quantities appearing in Equation (26) are given by Equations (10) and (14)–(17), but with $v_L = 0$. We have verified that Equation (26), when written in the atomic rest frame, is identical to the redistribution matrix derived by Landi Degl’Innocenti et al. (1997) based on the metalevel approach (see their Equation (15)). It is useful to note that in the non-magnetic case, we recover the Rayleigh phase matrix for a two-term atom without lower level polarization, but including J -state interference derived in Section 10.16 of LL04.

5. RESULTS AND DISCUSSIONS

To illustrate the general behavior of the redistribution matrix, we present the Stokes profiles resulting from a single 90° scattering event for an $L = 0 \rightarrow 1 \rightarrow 0$ scattering transition with $S = 1/2$. The J -quantum numbers of the lower and upper levels are $J_a = J_f = 1/2$ and $J_b = 1/2, 3/2$, which give rise to a doublet. Well-known examples of such doublets are the Na I D₁ and D₂, Ca II H and K, and Mg II h and k lines. The Na I D₁ and D₂ lines, in particular, are in addition affected by the presence of hyperfine structure, which would have to be taken into account for modeling purposes, but which is not dealt with here. Instead, a pair of hypothetical lines is used for the theoretical studies in the present paper. We study the influence of the field strength, the wavelength separation between the doublets, and the effect of a background continuum on the Stokes profiles. The magnetic field orientation is defined by angles ϑ_B and φ_B with respect to the polar z -axis (see Figure 1). For all the figures presented here, $\vartheta_B = 90^\circ$ and $\varphi_B = 45^\circ$. The incident radiation is assumed to be unpolarized ($[I_{\text{in}} = 1, 0, 0, 0]^T$) and spectrally flat (frequency independent). It is assumed to be incident in the vertical direction

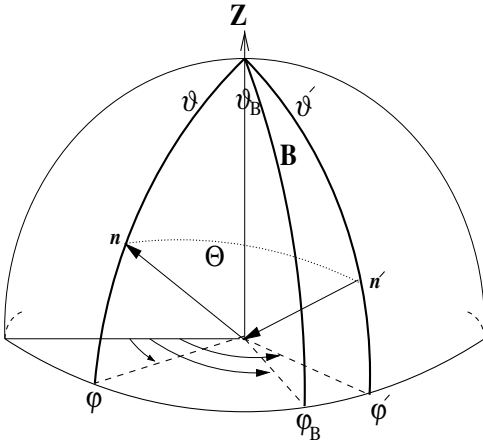


Figure 1. Illustration of the scattering geometry in a coordinate system where the magnetic field makes an angle ϑ_B with the polar z -axis and has an azimuth φ_B . (ϑ' , φ') refer to the incident ray and (ϑ , φ) to the scattered ray defined with respect to the z -axis. Θ is the scattering angle.

(parallel to the polar z -axis). Note that the PRD effects are contained in the redistribution matrix and manifest themselves irrespective of the spectral shape of the incident spectrum. The use of a flat spectrum is only a convenient choice.

The singly scattered Stokes vectors are then determined exclusively by the first column of the redistribution matrix. As

the elements of the redistribution matrix depend explicitly on λ and λ' , an integration over λ' is necessary to obtain the scattered Stokes profiles at λ . The magnetic field strength is parameterized by the splitting parameter ν_H given by

$$\nu_H = \frac{\lambda_0^2 e_0 B}{4\pi m c^2} \times \frac{1}{\Delta\lambda_D}, \quad (27)$$

where B is the field strength, e_0 is the charge of the electron, and m is its mass. $\Delta\lambda_D$ is the Doppler width. The radiative widths of both the lines are represented by a single damping parameter a , which is assumed to be 0.00143. The Doppler widths of both lines are 0.025 Å. Figures 2, 3, and 4 show I , Q/I , U/I , and V/I profiles for a range of field strengths and for three values of wavelength separations between the doublets. The positive Stokes Q directions for the incident and scattered beams lie on the respective meridian planes shown in Figure 1. If λ_1 and λ_2 denote the line center wavelengths of the two lines, then $\delta\lambda = |\lambda_1 - \lambda_2|$ denotes the separation between them. We have chosen $\delta\lambda = 6$ Å, 1 Å, and 0.1 Å, respectively, for Figures 2, 3, and 4. Different line types correspond to different values of ν_H . Note the characteristic signature of J -state interference in Q/I , namely, a polarization profile with two sign reversals, one between the two lines, the other at the center of the $J = 1/2 \rightarrow 1/2 \rightarrow 1/2$ transition line. In the absence of a background continuum, Q/I in the far wings approaches unity on both sides of the lines (see the solid line in the top left panel of Figure 9.2 in Stenflo 1994).

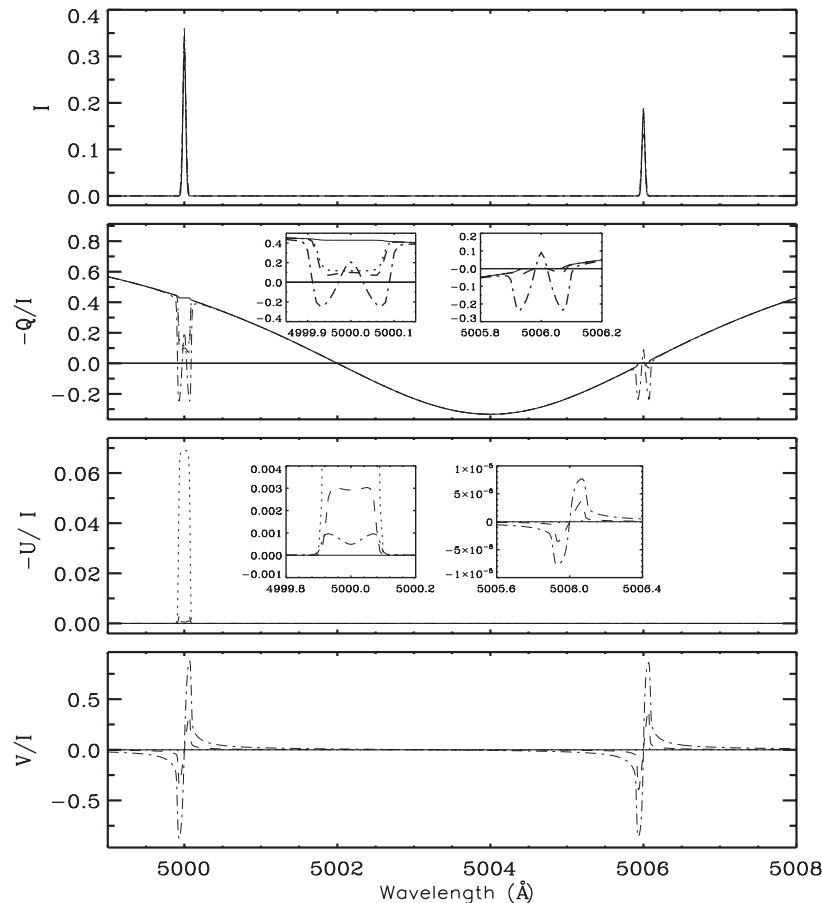


Figure 2. Profiles of the intensity I and the fractional polarizations Q/I , U/I , and V/I plotted for a hypothetical doublet at 5000 Å and 5006 Å with field-strength parameter $\nu_H = 0$ for the solid line, $\nu_H = 0.004$ for the dotted line, $\nu_H = 0.1$ for the dashed line, and $\nu_H = 0.5$ for the dash-dotted line. The fine-structure splitting is 6 Å. Single 90° scattering is assumed at the extreme limb ($\mu = 0$). The model parameters are $a = 0.00143$, $\vartheta_B = 90^\circ$, and $\varphi_B = 45^\circ$. The Doppler width $\Delta\lambda_D = 0.025$ Å. These profiles characterize scattering exclusively in the line pair without any background continuum.

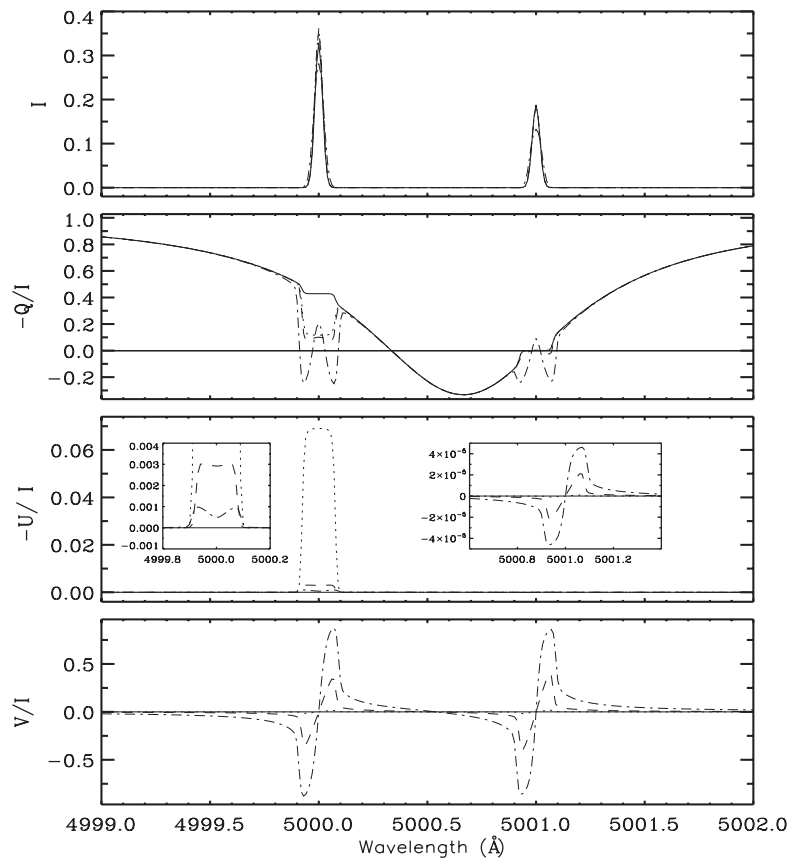


Figure 3. Same as Figure 2 except for the fine-structure splitting, which is 1 Å here. Note the shape of the U/I profiles (due to the increased magnitude of the J -state interference).

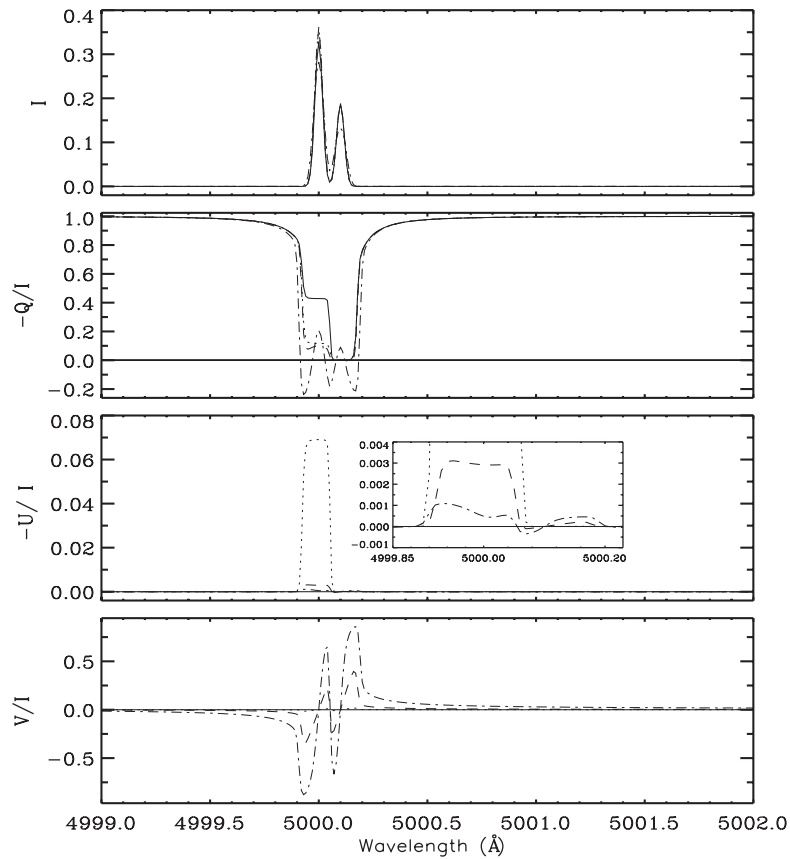


Figure 4. Same as Figure 2 except for the fine-structure splitting, which is now 0.1 Å. The polarization profiles overlap substantially, greatly enhancing the impact of the J -state interference.

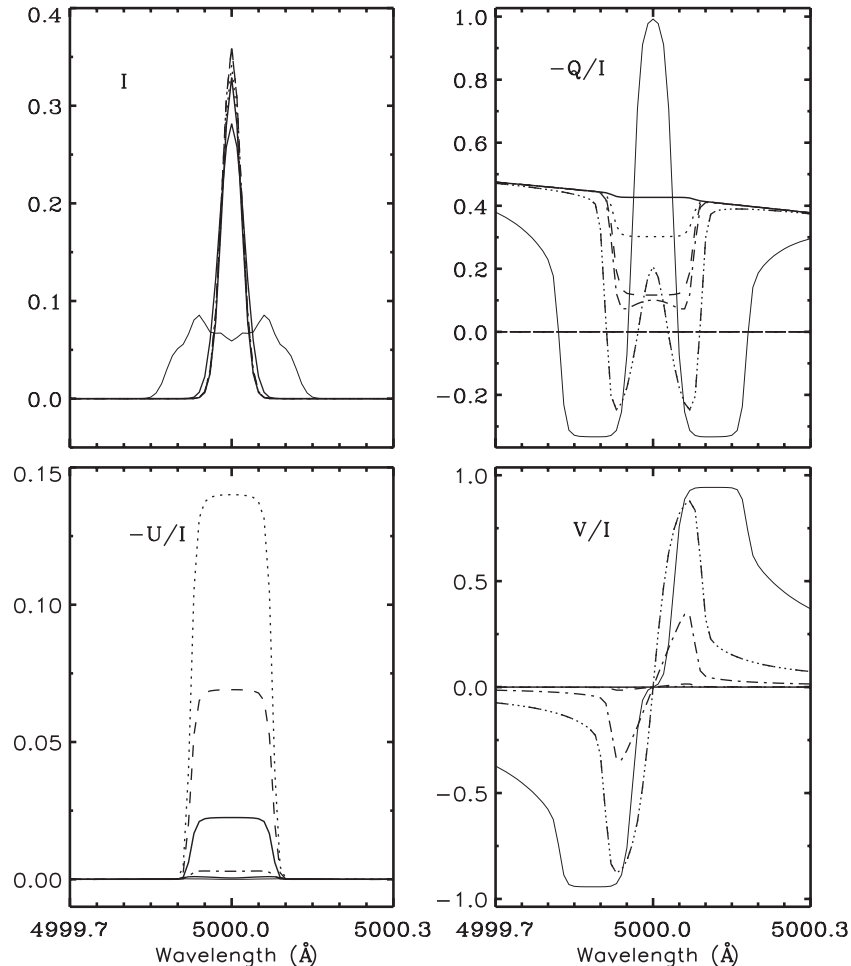


Figure 5. Profiles of the intensity I and the fractional polarizations Q/I , U/I , and V/I , plotted for a hypothetical line at 5000 \AA (of a line pair with the other line at 5006 \AA) with field-strength parameter $v_H = 0.00008$ for the solid line, $v_H = 0.0008$ for the dotted line, $v_H = 0.004$ for the dashed line, $v_H = 0.1$ for the dash-dotted line, $v_H = 0.5$ for the dash-triple-dotted line, and $v_H = 2.5$ for the thin solid line. Single 90° scattering is assumed at the extreme limb. The other model parameters are the same as in Figure 2. As before these profiles characterize scattering exclusively in the line without any background continuum.

The wavelength dependence of the J -state interference signature in the non-magnetic Q/I profile (based on the assumption of frequency coherent scattering in a doublet transition) is discussed in detail in Stenflo (1994). A wavelength-dependent depolarizability factor $W_2(\lambda)$ was introduced in that approach to conveniently describe the profile shape. In contrast, the present approach includes PRD in the doublet transition. The wavelength-dependent depolarizability of the line pair is implicitly built into the redistribution matrix. For the single scattering case presented in Figure 2, the Q/I profile computed with our PRD theory (solid line) gives results similar to the Q/I profile (solid line) in the top left panel in Figure 9.2 of Stenflo (1994).

In the weak field regime ($v_H = 0.004$), the shapes of the (Q/I , U/I) profiles are governed by the Hanle effect (depolarization in Q/I with respect to the non-magnetic case, and creation of a non-zero U/I signature). When the fields are sufficiently strong (for example, for $v_H = 0.1$), signatures of the transverse Zeeman effect show up in the cores of the two lines. In the core of the $J = 1/2 \rightarrow 1/2 \rightarrow 1/2$ transition line, the contribution from scattering polarization is zero (because $W_2 = 0$). As the field strength increases, one can clearly notice the characteristic Q/I profiles typical of the transverse Zeeman effect (see the dash-dotted lines in Figures 2, 3, and 4). The J -state interference (scattering) effects dominate the Q/I profiles outside the line cores.

As $\delta\lambda$ decreases, interesting signatures begin to show up in U/I more strongly (see the inset panels in Figures 2, 3, and 4). For the sake of discussion, let us consider the $\delta\lambda = 1 \text{ \AA}$ case. The signatures seen at the centers of both the lines at 5000 \AA and 5001 \AA for $v_H = 0.1$ and 0.5 appear to be entirely due to the J -state interference effects (because the contribution from the Zeeman effect to U is zero for the chosen geometry). However, the shapes of the U/I profiles are different from each other near the centers of the two lines. They can be understood in terms of the explicit expressions (not presented here) that have been derived for the case of the $L = 0 \rightarrow 1 \rightarrow 0$ scattering transition. Note that for the line separation 0.1 \AA (see Figure 4), the near-wings of the two lines overlap. This results in Q/I and U/I profiles with more complex shapes.

Extensive theoretical work and modeling of the J -state interference in the well-known D_1 and D_2 lines of Na I (including also the hyperfine structure and lower level polarization, but without PRD) have been carried out by Trujillo Bueno et al. (2002) and Casini & Manso Sainz (2005). Our emphasis in the present paper is to study the J -state interference effects in a hypothetical doublet when PRD effects are accounted for. In Figure 5 we show the effect of the magnetic field on the Stokes profiles in the core of the 5000 \AA line of the doublet for a wide range of field strengths. Here the doublet separation is chosen to be 6 \AA . Therefore, the J -state interference effect

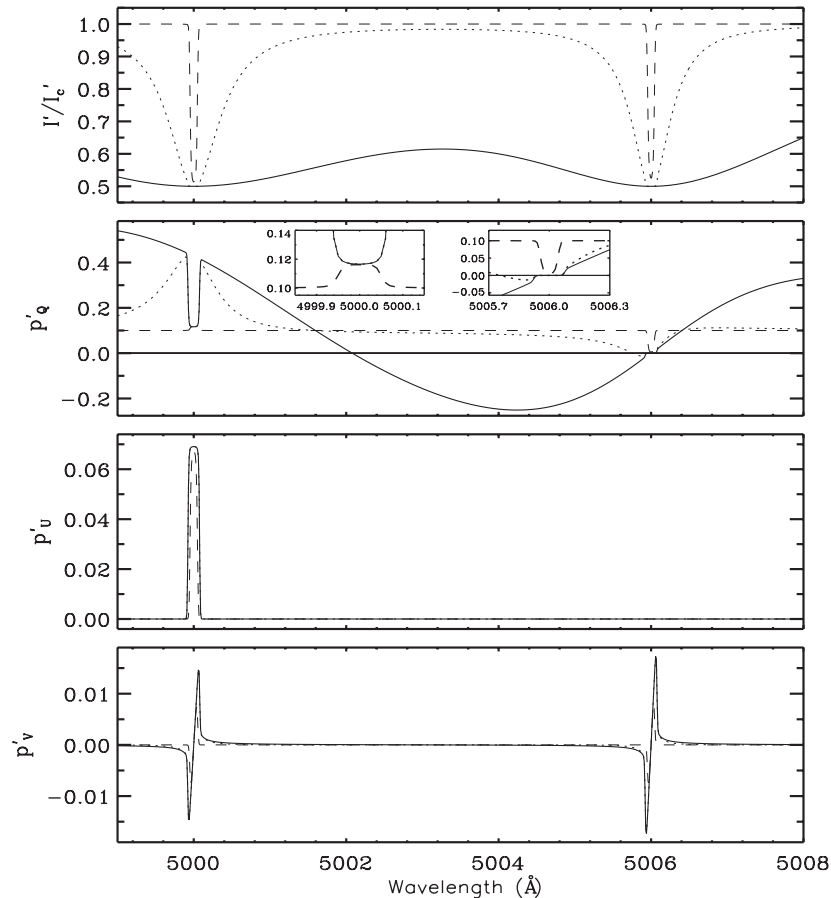


Figure 6. Profiles of the intensity I'/I'_c (see Equation (29)) and the fractional polarizations p'_Q , p'_U , and p'_V (see Equation (28)) plotted for the doublet at 5000 Å and 5006 Å in the presence of a background continuum. The field-strength parameter used is $v_H = 0.004$. Different strengths of the background continuum are represented by $c = 1 \times 10^{-8}$ for the solid line, 1×10^{-6} for the dotted line, and 1×10^{-2} for the dashed line. The limb-darkening parameter $\beta = 0.5$, and $b = 0.1$ for Q , while $b = 0$ for U and V . The other model parameters are the same as in Figure 2.

is extremely weak at the core of the line and shows up only in the wings (see the thick solid line in the Q/I panel). As the field strength increases from $v_H = 0.00008$ ($B \sim 0.1$ G) to $v_H = 2.5$ ($B \sim 4$ kG), the weak field Hanle scattering signatures make way for the strong field Zeeman signatures. The values of the Hanle Γ ($= \omega_L/\gamma$) parameter that correspond to the chosen set of v_H values are, respectively, 0.03, 0.28, 1.4, 7, 35, 175, and 874. For $\Gamma \leq 7$ the shapes of the polarization profiles are typical of the Hanle effect. For $\Gamma > 7$ we have entered the Zeeman regime, and the shapes of the polarization profiles become typical of the Zeeman effect. A comparison of Figure 5 for the $J = 1/2 \rightarrow 3/2 \rightarrow 1/2$ transition with Figure 3 of Stenflo (1998) for the $J = 0 \rightarrow 1 \rightarrow 0$ transition shows that the field-strength dependence is similar. Note that the $(a, \Delta\lambda_D) = (0.00143, 0.025 \text{ \AA})$ chosen by us is different from the corresponding values $(a, \Delta\lambda_D) = (0.004, 0.03 \text{ \AA})$ chosen in Stenflo (1998). Due to our choice of relatively smaller $(a, \Delta\lambda_D)$ values, we enter the Zeeman regime already for $v_H = 0.1$.

In the real solar spectrum the line emission is superposed on a background continuum that is weakly polarized. The relative importance of the line emission scales as $I/(I+c)$, where I is the line scattering probability and c is a constant representing the background continuum (see Stenflo 1998). The observed fractional polarization p' in the presence of a continuum is given by

$$p' = \frac{I}{(I+c)} p + \frac{c}{(I+c)} b, \quad (28)$$

where p is the fractional polarization given by $-Q/I$, $-U/I$, and V/I . b represents the continuum polarization (see Equation (58) in Stenflo 1998). In the presence of continuum, the Stokes I can be modeled by assuming LTE and using a Milne–Eddington model (see Stenflo 1998, for more details). With this assumption, one can show that (see Equation (61) of Stenflo 1998)

$$\frac{I'}{I'_c} = 1 - \beta + \frac{c}{(I+c)} \beta, \quad (29)$$

where β is the limb-darkening parameter, I' is the total intensity of scattered radiation, and I'_c is the intensity of the background continuum. Figures 6 and 7 show the Stokes profiles in the presence of a continuum for various values of c and for two values of v_H . Similar to Stenflo (1998), we choose the limb-darkening parameter $\beta = 0.5$ and continuum polarization $b = 0.1$ for Q and $b = 0$ for U and V . As the contributions from the background continuum increase, Stokes I takes the shape of a deep absorption line. The linear polarization Q/I approaches the continuum polarization level in the far wings. As the continuum parameter c increases from 10^{-8} to 10^{-2} , the J -state interference effects nearly vanish in the line wings. While the wings are dominated by the continuum polarization, the line core polarization is dominated by the Hanle or Zeeman effects depending on the field strength, irrespective of the strength of the background continuum. This can be seen from the inset figure in the Q/I panels of Figures 6 and 7.

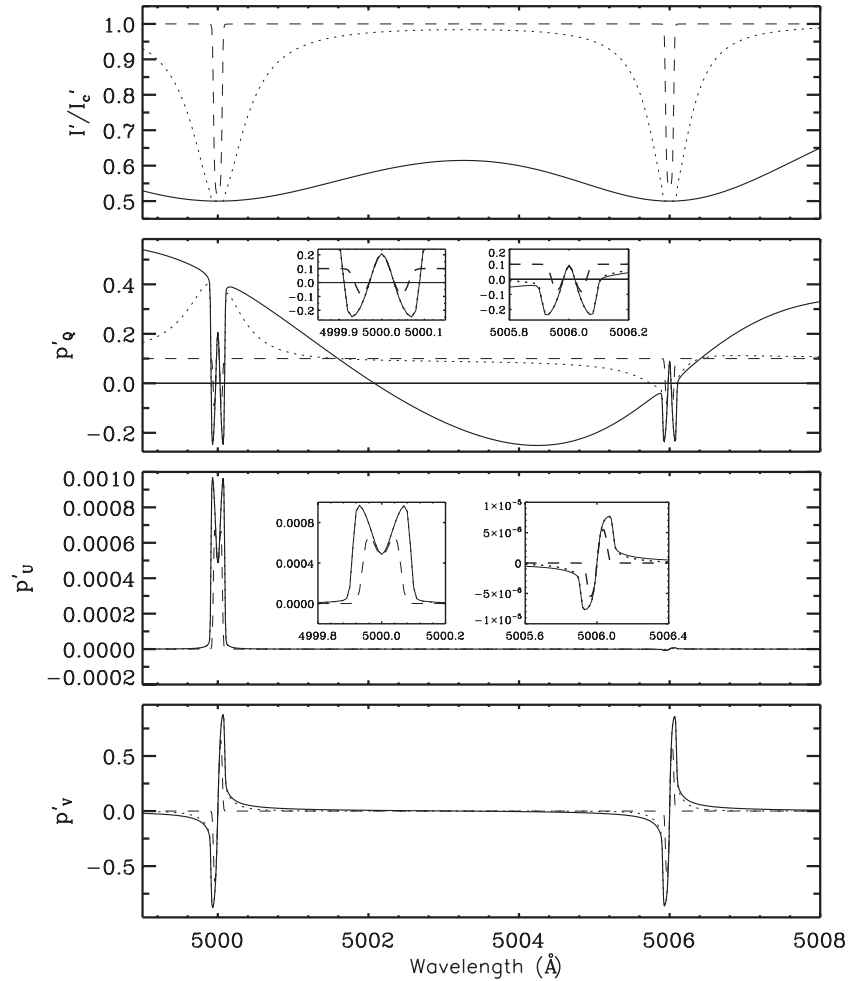


Figure 7. Same as Figure 6, but with $v_H = 0.5$, which represents a strong field regime ($B \sim 900$ G). The Zeeman effect dominates in the line cores. J -state interference effects are responsible for the shapes of $(Q/I, U/I)$ in the line wings.

6. CONCLUSIONS

We have derived a PRD matrix that includes J -state interference in a two-term atomic framework. The present treatment is limited to the collisionless regime and assumes that the Zeeman splitting is much smaller than the fine-structure splitting. With these restrictions we have derived laboratory frame expressions in the presence of magnetic fields of arbitrary strength and orientation (Hanle–Zeeman regime).

In the non-magnetic case we recover the collisionless PRD matrix derived by Landi Degl’Innocenti et al. (1997), who used a metalevel approach that can also treat J -state interference in the presence of a magnetic field. We also reproduce the results computed with the frequency coherent J -state interference theory of Stenflo (1994, 1997).

Examples of the Stokes profiles computed for the single scattering case are illustrated, with and without a background continuum. Due to the frequency coherent nature of the R^{II} function in the wings, the $(Q/I, U/I)$ profiles are quite similar to the corresponding profiles computed with the pure coherent scattering theory of Stenflo (1994). However, when the PRD matrices are used in radiative transfer computations, we expect to find significant differences with respect to the pure coherent scattering case, especially for optically thick lines.

As the fine-structure splitting decreases, the J -state interference effects show up in the line wings as well as the line cores. The shapes of the Stokes profiles depend strongly on the sepa-

ration of the doublet. Interesting signatures appear in the U/I profiles, particularly for strong fields.

M.S. is grateful to Drs. J. Trujillo Bueno and E. Landi Degl’Innocenti for useful discussions on the density matrix theory.

REFERENCES

- Bommier, V. 1997a, *A&A*, **328**, 706
 Bommier, V. 1997b, *A&A*, **328**, 726
 Bommier, V., & Sahal-Br  chot, S. 1978, *A&A*, **69**, 57
 Bommier, V., & Stenflo, J. O. 1999, *A&A*, **350**, 327
 Casini, R., & Manso Sainz, R. 2005, *ApJ*, **624**, 1025
 Chandrasekhar, S. 1950, *Radiative Transfer* (New York: Dover)
 Domke, H., & Hubeny, I. 1988, *ApJ*, **334**, 527
 Frisch, H. 2007, *A&A*, **476**, 665
 Hamilton, D. R. 1947, *ApJ*, **106**, 457
 Hummer, D. G. 1962, *MNRAS*, **125**, 21
 Landi Degl’Innocenti, E. 1983, *Sol. Phys.*, **85**, 3
 Landi Degl’Innocenti, E. 1984, *Sol. Phys.*, **91**, 1
 Landi Degl’Innocenti, E. 1985, *Sol. Phys.*, **102**, 1
 Landi Degl’Innocenti, E., Landi Degl’Innocenti, M., & Landolfi, M. 1997, in *Proc. Forum TH  MIS, Science with TH  MIS*, ed. N. Mein & S. Sahal-Br  chot (Paris: Obs. Paris-Meudon), 59
 Landi Degl’Innocenti, E., & Landolfi, M. 2004, *Polarization in Spectral Lines* (Dordrecht: Kluwer) (LL04)
 Omont, A., Smith, E. W., & Cooper, J. 1972, *ApJ*, **175**, 185
 Omont, A., Smith, E. W., & Cooper, J. 1973, *ApJ*, **182**, 283
 Sampoorna, M. 2011, *ApJ*, **731**, 114

- Sampoorna, M., Nagendra, K. N., & Stenflo, J. O. 2007a, [ApJ](#), **663**, 625 (P1)
- Sampoorna, M., Nagendra, K. N., & Stenflo, J. O. 2007b, [ApJ](#), **670**, 1485 (P2)
- Stenflo, J. O. 1978, *A&A*, **66**, 241
- Stenflo, J. O. 1980, *A&A*, **84**, 68
- Stenflo, J. O. 1994, *Solar Magnetic Fields: Polarized Radiation Diagnostics* (Dordrecht: Kluwer)
- Stenflo, J. O. 1997, *A&A*, **324**, 344
- Stenflo, J. O. 1998, *A&A*, **338**, 301
- Stenflo, J. O., & Keller, C. U. 1996, *Nature*, **382**, 588
- Stenflo, J. O., & Keller, C. U. 1997, *A&A*, **321**, 927
- Trujillo Bueno, J., Casini, R., Landolfi, M., & Landi Degl'Innocenti, E. 2002, [ApJ](#), **566**, L53